ICAMT 2004
Kuala Lumpur, 11-13 May 2004

MODELING OF PIEZOELECTRIC LAMINATED COMPOSITE PLATE USING FINITE ELEMENT ANALYSIS

Iskandar Al-Thani Mahmood[a] **and Md. Raisuddin Khan**[b]
Department of Mechatronics Engineering, Faculty of Engineering
International Islamic University Malaysia, Kuala Lumpur, Malaysia
(Email: [a]am.iskandar@iiu.edu.my and [b]raisuddin@iiu.edu.my)

Abstract

A finite element model for shape control analysis of piezoelectric laminated composite plate is presented in this paper. Elastic field and electric field of the piezoelectric laminated composite plate has been coupled through the linear piezoelectric constitutive equations. Piezoelectric actuators and sensors are modeled as additional layers either to be surface bonded or embedded in the laminated composite plate. A computer code was written in C++ based on the finite element model and was successfully validated with experimental and numerical results that are readily available in the literatures. The effects of actuator voltage, actuator orientation, fiber orientation and actuator placement along the thickness direction have been simulated and analyzed using the present model.

Keyword: piezoelectric; composites; smart structures.

1. Introduction

The needs for structures with self-monitoring and self-controlling capabilities especially in aerospace applications have caused remarkable growth in the research and development of smart structures. A smart structure can be defined as a structure made up of purely elastic materials, called the substrate, integrated with surface mounted or embedded sensors and actuators that have the capability to sense and take corrective action [11]. In the present research, to make up the smart structure, piezoelectric material that has the capabilities to act as actuators and sensors due to direct and converse piezoelectric effect is chosen to be integrated into a laminated composite plate. The direct piezoelectric effect is the ability to generate electrical charge in proportion to externally applied mechanical force, and the converse piezoelectric effect is exactly the inverse of the direct effect. Laminated composite plate is chosen as the substrate for its high strength-to-weight and stiffness-to-weight ratios [5]. These characteristics make the laminated composite plate suitable to be used in many applications especially in aerospace applications.

There are numerous exact solutions developed to describe the kinematic behavior of the piezoelectric laminated composite plates. However, exact solution becomes very difficult to obtain when the configuration of the structures with piezoelectric laminates embedded becomes complex. An alternative solution would be to use finite element solutions. The work of Allik and Hughes [1] can be considered as one of the pioneer in the field of finite element formulation, which includes piezoelectric effects in structures. A two-dimensional quadrilateral piezoelectric plate element with one electrical degree of freedom per element was developed by Hwang and Park [4] to study vibration control of a piezoelectric laminated composite plate. The plate element has four nodes and each of the nodes has three mechanical degrees of freedom. Classical laminated plate theory (CLPT) with induced strain actuation and Hamilton's principle were used to formulate the equation of motions. It was found active and passive control affect each other, thus should be considered simultaneously in designing efficient controlled structures.

The works done using CLPT were found only suitable to model thin plate. However to model thick plate, it is generally accepted that higher-order shear displacement theory (HSDT) can model more accurately, since through HSDT effect of transverse shear stresses are captured. Ray et. al. [9] developed a finite element model for static analysis of a simply supported rectangular intelligent plate using the HSDT. An eight-noded two-dimensional quadratic quadrilateral isoparametric element was derived to model the coupled electromechanical behavior. The results obtained in these work were compared with exact solutions done by the same authors previously [8] and found to be in good agreement. Chattopadhyay and Seeley [2] developed a refined HSDT and used finite element method to analyze laminated composite plate surface bonded or embedded with piezoelectric layers. Non-linearities were introduced to the problem through the strain dependent piezoelectric strain coefficients and the assumed strain distribution through the thickness. Results obtained from this model were shown to agree well with published experimental results by Crawley and Lazarus [3].

In the present research, the HSDT developed by Pervez [7] is used in order to accurately describe the kinematic behavior of the laminated composite plates and the piezoelectric layers. The elastic field and the electric field are coupled through the linear piezoelectric constitutive equations. In the finite element model, an eight-noded two-dimensional isoparametric element is used. Each node has seven mechanical degrees of freedom and one electrical degree of freedom. The present model is validated

with experimental and numerical results that are readily available in the literatures.

2. Kinematics and constitutive relationships

Figure (2.1) shows the geometry of the laminated composite plate surface bonded with piezoelectric actuator layer on the top and bottom. The plate of total thickness *h*, length *a*, width *b* has *n* number of layers.

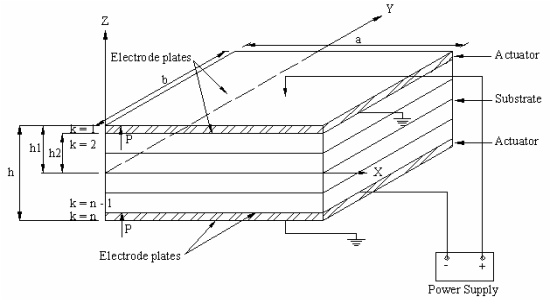

Figure 2.1: Plate configuration

The higher-order shear displacement fields considered in this research work are [7]:

$$u(x,y,z,t) = u_o(x,y,t) + z\theta_x + z^3\zeta_x \quad (2.1a)$$

$$v(x,y,z,t) = v_o(x,y,t) + z\theta_y + z^3\zeta_y \quad (2.1b)$$

$$w(x,y,z,t) = w_o(x,y,t) \quad (2.1c)$$

where *u, v, w* are the displacements of a generic point (*x, y, z*) in *x, y* and *z* directions respectively; u_o, v_o, w_o are the displacements of mid-plane in *x, y* and *z* direction respectively; *z* is the coordinate in thickness direction; θ_x, θ_y are the rotations of normals to reference surface about the *y* and *x* axes respectively; and ζ_x, ζ_y are the third order displacements or warping functions.

The strain associated with the displacement fields can be expressed as follows [13]:

$$\{\varepsilon\} = \left[Z'\right]\{\bar{\varepsilon}\} \quad (2.2a)$$

where,

$$\{\varepsilon\} = \{\varepsilon_{xx}\ \ \varepsilon_{yy}\ \ \gamma_{yz}\ \ \gamma_{xz}\ \ \gamma_{xy}\}^T \quad (2.2b)$$

$$\{\bar{\varepsilon}\} = \left[\frac{\partial u_o}{\partial x}\ \frac{\partial v_o}{\partial y}\ \frac{\partial \theta_x}{\partial x}\ \frac{\partial \theta_y}{\partial y}\ \frac{\partial \zeta_x}{\partial x}\ \frac{\partial \zeta_y}{\partial y}\ \theta_y + \frac{\partial w_o}{\partial y}\ 3\zeta_y\ \theta_x + \frac{\partial w_o}{\partial x}\ 3\zeta_x\ \frac{\partial u_o}{\partial y} + \frac{\partial v_o}{\partial x}\ \frac{\partial \theta_x}{\partial y} + \frac{\partial \theta_y}{\partial x}\ \frac{\partial \zeta_x}{\partial y} + \frac{\partial \zeta_y}{\partial x}\right]^T \quad (2.2c)$$

$$\left[Z'\right] = \begin{bmatrix} 1 & 0 & z & 0 & z^3 & 0 & 0 & 0 & 0 & 0 & 0 & 0 & 0 \\ 0 & 1 & 0 & z & 0 & z^3 & 0 & 0 & 0 & 0 & 0 & 0 & 0 \\ 0 & 0 & 0 & 0 & 0 & 0 & 1 & z^2 & 0 & 0 & 0 & 0 & 0 \\ 0 & 0 & 0 & 0 & 0 & 0 & 0 & 0 & 1 & z^2 & 0 & 0 & 0 \\ 0 & 0 & 0 & 0 & 0 & 0 & 0 & 0 & 0 & 0 & 1 & z & z^3 \end{bmatrix} \quad (2.2d)$$

where $\varepsilon_{xx}, \varepsilon_{yy}$ and γ_{xy} are the in plane strain components. γ_{yz} and γ_{xz} are the transverse shear strain components.

In the present research, quasi-static loading and plane stress formulations are assumed. The constitutive equations for *k*th orthotropic layers expressed in the material coordinate system are given as follows:

$$\begin{Bmatrix} \sigma_1 \\ \sigma_2 \\ \sigma_{23} \\ \sigma_{13} \\ \sigma_{12} \end{Bmatrix}^k = \begin{pmatrix} Q_{11} & Q_{12} & 0 & 0 & 0 \\ Q_{12} & Q_{22} & 0 & 0 & 0 \\ 0 & 0 & R_{44} & 0 & 0 \\ 0 & 0 & 0 & R_{55} & 0 \\ 0 & 0 & 0 & 0 & Q_{66} \end{pmatrix}^k \begin{Bmatrix} \varepsilon_1 \\ \varepsilon_2 \\ \gamma_{23} \\ \gamma_{13} \\ \gamma_{12} \end{Bmatrix}^k \quad (2.3)$$

For the piezoelectric layers, the linear piezoelectric constitutive equations that couples the elastic field and electric field are given as follows:

$$\begin{Bmatrix} \sigma_1 \\ \sigma_2 \\ \sigma_{23} \\ \sigma_{13} \\ \sigma_{12} \end{Bmatrix}^k = \begin{pmatrix} Q_{11} & Q_{12} & 0 & 0 & 0 \\ Q_{12} & Q_{22} & 0 & 0 & 0 \\ 0 & 0 & R_{44} & 0 & 0 \\ 0 & 0 & 0 & R_{55} & 0 \\ 0 & 0 & 0 & 0 & Q_{66} \end{pmatrix}^k \begin{Bmatrix} \varepsilon_1 \\ \varepsilon_2 \\ \gamma_{23} \\ \gamma_{13} \\ \gamma_{12} \end{Bmatrix}^k - \begin{pmatrix} 0 & 0 & e_{31} \\ 0 & 0 & e_{32} \\ 0 & e_{24} & 0 \\ e_{15} & 0 & 0 \\ 0 & 0 & 0 \end{pmatrix}^k \begin{Bmatrix} E_1 \\ E_2 \\ E_3 \end{Bmatrix}^k \quad (2.4a)$$

$$\begin{Bmatrix} D_1 \\ D_2 \\ D_3 \end{Bmatrix}^k = \begin{pmatrix} 0 & 0 & 0 & e_{15} & 0 \\ 0 & 0 & e_{24} & 0 & 0 \\ e_{31} & e_{32} & 0 & 0 & 0 \end{pmatrix}^k \begin{Bmatrix} \varepsilon_1 \\ \varepsilon_2 \\ \gamma_{23} \\ \gamma_{13} \\ \gamma_{12} \end{Bmatrix}^k + \begin{pmatrix} p_{11} & 0 & 0 \\ 0 & p_{22} & 0 \\ 0 & 0 & p_{33} \end{pmatrix}^k \begin{Bmatrix} E_1 \\ E_2 \\ E_3 \end{Bmatrix}^k \quad (2.4b)$$

The electric fields are given as [10]:

$$\begin{Bmatrix} E_{xx} \\ E_{yy} \\ E_{zz} \end{Bmatrix}^k = -\begin{Bmatrix} \frac{\partial \phi}{\partial x} \\ \frac{\partial \phi}{\partial y} \\ \frac{\partial \phi}{\partial z} \end{Bmatrix}^k \quad (2.5)$$

where ϕ^k is the electric potential. The electric potential is assumed to have linear variations across the thickness of the actuator/sensor layers as:

$$\phi^k(x,y,z)=\frac{z-h_{k+1}}{h_k-h_{k+1}}\phi_o^k(x,y) \qquad (2.6)$$

where ϕ_o^k can be treated as the generalized electric potential similar to the generalized displacement at any point on the surface of the actuator and the sensor layers.

3. Finite element formulation

The overall plate is meshed into a finite number of elements by an eight-noded two-dimensional isoparametric element. Referring to Equation (2.1), the generalized displacement vector for node i (i=1,2,…..,8) of the element can be written as:

$$\{u_i\}=\{u_{oi}\ \ v_{oi}\ \ w_{oi}\ \ \theta_{xi}\ \ \theta_{yi}\ \ \zeta_{xi}\ \ \zeta_{yi}\}^T \qquad (3.1)$$

From the above equation, the nodal generalized displacement vector of a typical eight-noded element *e* can be expressed as:

$$\{u^e\}=\{(u_1)^T\ \ (u_2)^T\ \ .....\ \ (u_7)^T\ \ (u_8)^T\}^T \qquad (3.2)$$

Thus, the generalized displacement vector at any point within the element can be obtained by interpolating the nodal generalized displacement as:

$$\{u\}=[N]\{u^e\} \qquad (3.3a)$$

where the shape function matrix is given as:

$$[N]=[[N_1]\ [N_2]\ .....\ [N_7]\ [N_8]] \qquad (3.3b)$$

and $[N_i]=n_i[I]$. Here $[I]$ is an identity matrix of size 7x7 and $n_i(i=1,2,3.....,8)$ is the shape function of natural coordinates (ζ,η) associated with the *i*th node [10].

Referring to Equation (2.2a), by substituting Equation (3.3a) the generalized strain vector $\{\bar{\varepsilon}\}$ at any point within the element can be express as:

$$\{\bar{\varepsilon}\}=[B]\{u^e\} \qquad (3.4a)$$

where the nodal strain-displacement matrix is given as:

$$[B]=[[B_1]\ [B_2]\ .....\ [B_7]\ [B_8]] \qquad (3.4b)$$

The elements of each submatrix $[B_i]$ of $[B]$ are given explicitly in Mahmood [6].

Similarly, electric potential can also be generalized at any point within the element as:

$$\{\phi_o^k\}=[N_p]\{\phi_o^{ke}\} \qquad (3.5a)$$

where,

$$\{\phi_o^{ke}\}=\{\phi_{o1}^{ke}\ \ \phi_{o2}^{ke}\ .....\ \phi_{o7}^{ke}\ \ \phi_{o8}^{ke}\}^T \qquad (3.5b)$$

$$[N_p]=[N_1\ \ N_2\ .....\ N_7\ \ N_8] \qquad (3.5c)$$

and $\{\phi_{oi}^{ke}\}(i=1,2.....8)$ is the electric potential at the *i*th node.

Using Equation (3.5a) electric filed in the Equation (2.5) can be written as follows:

$$\{E^k\}=[Z_p^k][B_p]\{\phi_o^{ek}\} \qquad (3.6a)$$

where, $[Z_p^k]$ and $[B_p]$ are given explicitly in Mahmood [6].

Variation principle in conjunction with Equation (3.1) to (3.6) yields the following two sets of matrix equations:

$$[K_{uu}^e]\{u^e\}+[K_{u\phi}^e]\{\phi_o^{ek}\}=\{F_S^e\} \qquad (3.7a)$$

$$[K_{\phi u}^e]\{u^e\}+[K_{\phi\phi}^e]\{\phi_o^{ek}\}=\{Q_S^e\} \qquad (3.7b)$$

where,

$$[K_{uu}^e]=\int_{-1}^{+1}\int_{-1}^{+1}[B]^T\left(\sum_{k=1}^{k=n}\int_{h_{k+1}}^{k}[Z']^T[\bar{Q}][Z']dz\right)[B]\det J d\varsigma d\eta \qquad (3.7c)$$

$$[K_{u\phi}^e]=\int_{-1}^{+1}\int_{-1}^{+1}[B]^T\left(\sum_{k=1}^{k=n}\int_{h_{k+1}}^{k}[Z']^T[\bar{e}][Z_p^k]dz\right)[B_p^k]\det J d\varsigma d\eta \qquad (3.7d)$$

$$[K_{\phi u}^e]=\int_{-1}^{+1}\int_{-1}^{+1}[B_p^k]^T\left(\sum_{k=1}^{k=n}\int_{h_{k+1}}^{k}[Z_p^k]^T[\bar{e}][Z']dz\right)[B]\det J d\varsigma d\eta \qquad (3.7d)$$

$$[K_{\phi\phi}^e]=\int_{-1}^{+1}\int_{-1}^{+1}[B_p^k]^T\left(\sum_{k=1}^{k=n}\int_{h_{k+1}}^{k}[Z_p^k]^T[\bar{p}][Z_p^k]dz\right)[B_p^k]\det J d\varsigma d\eta \qquad (3.7c)$$

$$[F_S^e]=\iint_{S1}[N]^T[Z]_{z=h1}^T\{\bar{T}\}dS \qquad (3.7e)$$

$$[Q_S^e]=\iint_{S2}[N_p]^T\{\bar{q}'\}dS \qquad (3.7f)$$

where $[K_{uu}^e]$ is the elastic stiffness matrix, $[K_{u\phi}^e]=[K_{\phi u}^e]^T$ is the coupling stiffness matrix between mechanical and electrical effects, $[K_{\phi\phi}^e]$ is the dielectric stiffness matrix, $[F_S^e]$ is the mechanical force as a result of the surface force and $[Q_S^e]$ is the electric force as a result of the applied surface charge on the actuators.

For open-loop shape control, Equation (3.7a) is rearranged as follows:

$$[K_{uu}]\{\mathbf{U}\}=\{F_S\}-\{F_{act}\} \qquad (3.8)$$

where $\{F_{act}\}=[K_{u\phi}]\{\mathbf{\Phi}\}$ is an additional force due to the voltage $\{\mathbf{\Phi}\}$ applied to the actuator layer and $\{F_S\}$ is the mechanical force.

4. Results and discussions

The section begins with validations of the finite element formulation and the code written for this research.

4.1. Validations

Validation was based on experiment conducted by Tzou [12]. The experiment used a cantilevered piezoelectric bimorph beam as shown in Figure (4.1).

It consisted of two bonded layers of PVDF. The beam has total thickness h = 0.001 m, length a = 0.1 m and width b = 0.005 m. The top and bottom surface of the beam were subjected to an electrical potential of 1.0 V across the thickness of the beam.

The difference in the electric polarity between the piezoelectric layers caused the bottom and top layer to expand and contract respectively in the transverse direction. As a result, the beam bends upward and the corresponding displacements were measured. The results from the present model are shown in Table (4.1). The present results give an excellent correlation with other results especially with Tzou's theoretical solutions.

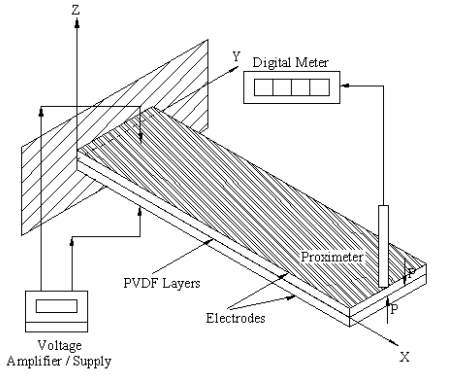

Figure (4.1): Experimental setup for piezoelectric bimorph as conducted by Tzou [12].

Table (4.1): Deflection along length of the bimorph beam.

Location x (mm)	Deflections (x 10^{-7} m)				
	20	40	60	80	100
Experimental[a]	-	-	-	-	3.15
Theory[a]	0.138	0.552	1.24	2.21	3.45
FEM[a]	0.124	0.508	1.16	2.10	3.30
FEM[b]	0.139	0.553	1.24	2.21	3.45

[a]Tzou [12]; [b]Present

In order to validate the sensing capability of piezoelectric structure, another validation was performed based on the numerical simulation of the bimorph beam done by Tzou et. al. (data taken from Hwang and Park [4]). The tip of the bimorph beam was deflected by a distance of 10.0 mm and the generated voltage differences across the top and bottom layers of the bimorph beam were determined and plotted in Figure (4.2).

In Tzou et. al.'s works, the sensor voltage on the bimorph beam is modeled as though there are several point electrodes placed along the beam. As seen in the Figure (4.2), it has resulted in a continuous voltage output along the beam. In the model of Hwang and Park [4], an electrode plate is used to cover each element that is five identical electrodes along the bimorph beam. The present results for this sensing capability agree very well with existing results by Tzou et. al. and Hwang and Park [4].

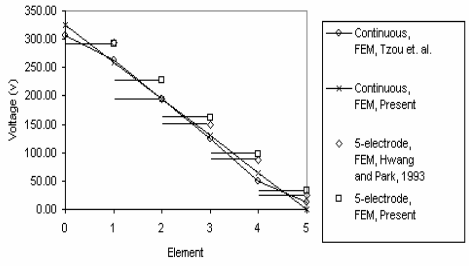

Figure (4.2): Voltage difference across the thickness of the bimorph beam.

4.2. Numerical simulations

After successfully validating the formulation and the code, various numerical simulations were done to investigate the influence of piezoelectric actuator on shape of the piezoelectric laminated composite plates. Three types of materials are used in the present numerical simulations. There are T300/976 graphite/epoxy, PZT Fibers and piezoceramic G1195 [6]. Unless specified otherwise, $[0^0/90^0/90^0/0^0]$ cross-ply symmetric laminated plate is considered with one layer of piezoceramic PZT-G1195 bonded on the top and bottom surface. In addition, unless specified otherwise when the present research states that a constant voltage of 300 V is applied to the piezoceramic layers, it means that +300 V and –300 V is applied to the surface of the top and bottom piezoceramic layers respectively.

4.2.1. Effects of actuator voltage on symmetric cross-ply laminates

The shape of a cantilever plate under different actuator voltages that are applied to the piezoceramic layers are presented in Figure (4.3a & b). The figures show the plate deflection increases as the actuator voltage increases. Figure (4.3b) shows the shape of cantilever plate at the plate's free end. It can be seen as the actuator voltage increases, the degree of curvature formed at plate's free end also increased.

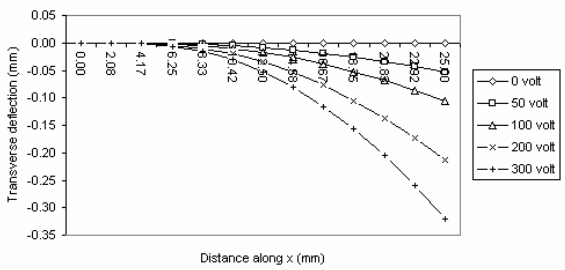

Figure (4.3a): Effect of different actuator voltage on centerline (y = b/2) deflection.

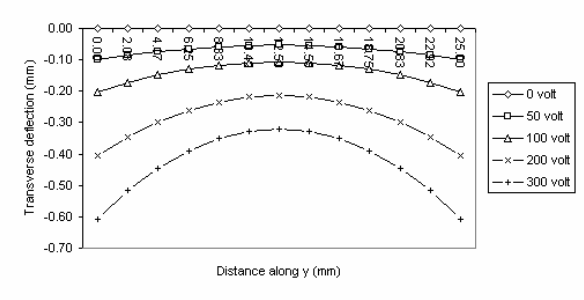

Figure (4.3b): Effect of different actuator voltage on free end (x = a) deflection.

4.2.2. Effects of different fiber orientation

The effects of different fiber orientation on the shape of cantilever plate under a constant actuator voltage of 300 V are shown in Figure (4.4a & b). The fiber orientations are varied from 0 to 45 degrees. It is seen in Figure (4.4a) the increase in fiber orientation increases the centerline deflection.

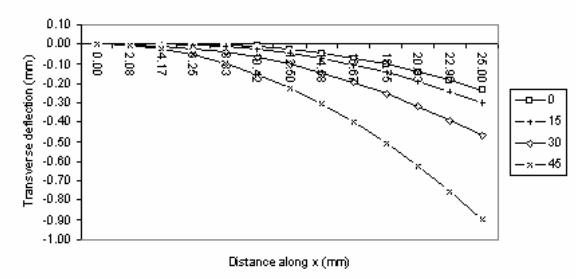

Figure (4.4a): Effect of different fiber orientations (-θ.θ.-θ.θ) on centerline (y = b/2) deflection under constant actuator voltage of 300 V.

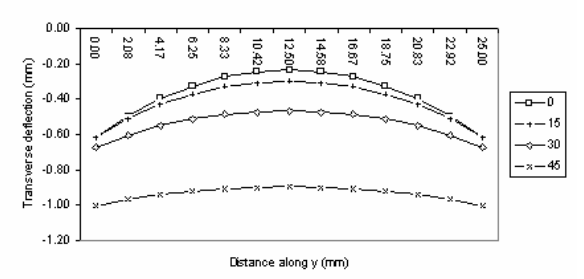

Figure (4.4b): Effect of different fiber orientations (-θ.θ.-θ.θ) on free end (x = a) deflection under constant actuator voltage of 300 V.

Note that there is significant increase in the maximum deflection when the fiber orientation is incremented from 0 to 45 degrees. It is also noticed in Figure (4.4b) that increase in fiber orientation reduces curvature at the free end, and at 45 degrees, the free end becomes almost flat.

4.2.3. Effects of actuator orientation on symmetric cross-ply laminates

The effect of actuator orientation is analyzed in this section by rotating the actuators along the *z*-axis. In order to see the effect of actuator orientation, uni-axial piezoceramic PZT Fibers are used.

Figure (4.5a & b) present the effect of actuator orientation on a cantilever plate under actuator voltage of 300 V. The shape of the plate changed considerably when the actuator angle is changed from 0 to 90 degrees. At 0 degree, the top and bottom piezoceramic layers expand and contract in the *x* direction. This caused the plate to bend downwards. However, at 90 degrees, the expansions and contractions occur in the *y* direction which caused the plate to bend upwards.

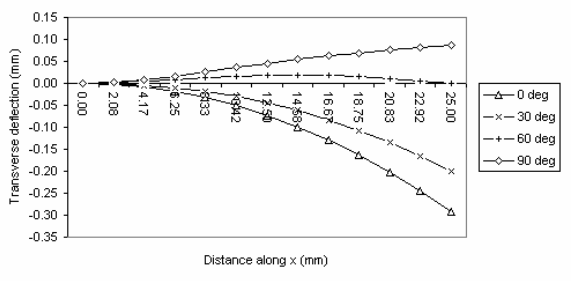

Figure (4.5a): Effect of actuator orientation on centerline (y = b/2) deflection under constant actuator voltage of 300 V.

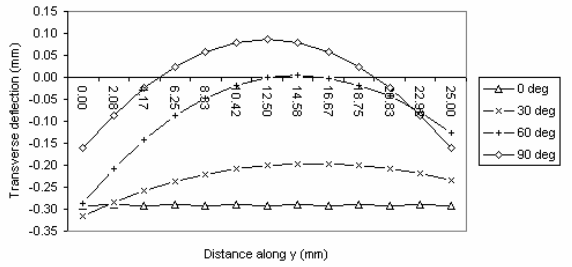

Figure (4.5b): Effect of actuator orientation on free end (x = a) deflection under constant actuator voltage of 300 V.

4.2.4. Effects actuator placement along the thickness direction on symmetric cross-ply laminates

The placements of actuators are varied across the thickness of a composite laminated plate and a constant voltage of 300 V is applied to the actuators. The shape of a cantilever plate under these conditions is presented in Figure (4.6a & b). The figures show maximum deflection is achieved when the actuators are placed at the outer layers of the plate. As the actuators are brought closer to the middle plane, the deflection that caused by the actuators diminishes. The plate behaves in this manner because as the actuators are brought closer to the middle plane, the moments generated by the actuators are reduced. The deflection also diminishes if the actuators are placed next to each other as illustrated in $[P/P/0^0/90^0/90^0/0^0]$ laminate configuration. This is because of the moments generated by the top actuator are canceled by the moments generated by the bottom actuator.

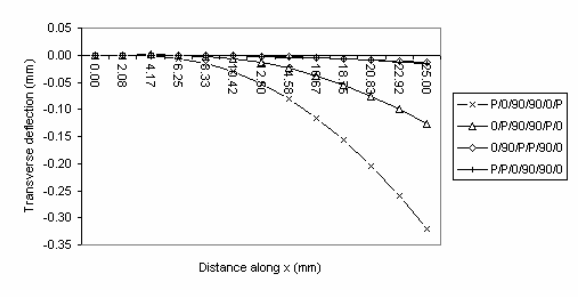

Figure (4.6a): Effect of through thickness actuator placement on centerline (y = b/2) deflection under constant actuator voltage of 300 V.

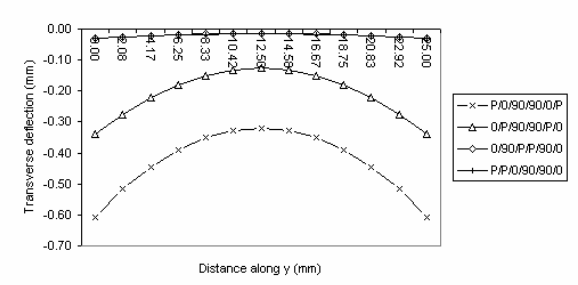

Figure (4.6b): Effect of through thickness actuator placement on free end (x = a) deflection under constant actuator voltage of 300 V.

5. Conclusions

Study of the behavior of piezoelectric laminated composite plates using HSDT shows promising results. The behavior of a piezoelectric laminated cantilever plate studied in this research shows that:

1. Increasing the actuator voltage increases plate deflection at the free end. However, the free end is found to become curve about the longitudinal axis.
2. By orientating the fiber at [$-45^0/45^0/-45^0/45^0$] anti-symmetric angle ply, a similar deflection shape as the one produced by a uni-axial piezoelectric material can be produced by a bi-axial piezoelectric material on a cantilever plate, where the curvature that usually formed at the plate's free end can be eliminated.
3. It was found that the actuators are most effective when placed on the outer layer of the plates. The effectiveness of the actuators vanishes as they are placed closer to the middle plane or if they are placed next to each other.

References

1. Allik, H. and Hughes, T.J.R. 1970. Finite element method for piezoelectric vibration. *International Journal for Numerical Methods in Engineering* 2: 151-157.
2. Chattopadhyay, A. and Seeley, E.S. 1997. A higher order theory for modeling composite laminates with induced strain actuators. *Composites Part B 28B*: 243-252.
3. Crawley, E.F. and Lazarus, K.B. 1991. Induced strain actuation of isotropic and anisotropic plates. *AIAA Journal 29(6)*: 944-951.
4. Hwang, W. -S. and Park, H. C. 1993. Finite element modeling of piezoelectric sensors and actuators. *AIAA Journal 31(5)*: 930-937.
5. Jones, M.R. 1975. *Mechanics of composite materials*. Cambridge: Cambridge University Press.
6. Mahmood, I.A. 2003. Shape Control Analysis of Piezoelectric Laminated Composite Plate using Finite Element Method. M.Sc. Thesis. International Islamic University Malaysia, Malaysia.
7. Pervez, T. 1991. Transient dynamics, damping and elasto-plastic analysis of higher order laminated anisotropic composite plates using finite element method. Ph.D. Thesis. University of Minnesota, USA.
8. Ray, M.C., Bhattacharya, R. and Samanta, B. 1993. Exact solutions for analysis of intelligent structures. *AIAA Journal* 31(9): 1684-1691.
9. Ray, M.C., Bhattacharyya, R. and Samanta, B. 1994. Static analysis of an intelligent structure by the finite element method. *Computers and Structures 52(4)*: 617-631.
10. Ray, M.C., Samanta, B. and Bhattacharyya, R. 1996. Finite element model for active control of intelligent structures. *AIAA Journal 34(9)*: 1885-1893.
11. Reddy, J.N, 1999. On laminated plates with integrated sensors and actuators. *Engineering Structures 21*: 568-593.
12. Tzou, H.S. 1993. *Piezoelectric shells distributed sensing and control of continua*. KAP, Norwell, MA.
13. Ugural, A.C. 1981. *Stress in plates and shells*. New York: McGraw-Hill Book Company.

6. Appendix A. Material properties

Table (4.1): Material and geometrical properties used in this research
(data from [1]Correia et. al. 2000; [2]Gosh and Batra 1995; [3]Reddy and Pandey 1987; [4]Rabinovitch et. al. 2002).

Properties	**Aluminum alloy[1]**	**S-glass/ Epoxy[1]**	**T300/976[2]**	**T300/5208[3]**	**PVDF [1]**	**PXE-5[1]**	**PZT-G1195[2]**	**PZT Fibers[4]**
Elastic modulus, E_1	69.0 x 10^9 Pa	55.0 x 10^9 Pa	150.0 x 10^9 Pa	19.2 x 10^6 psi	2.0 x 10^9 Pa	66.6 x 10^9 Pa	63.0 x 10^9 Pa	
Elastic modulus, E_2	69.0 x 10^9 Pa	16.0 x 10^9 Pa	9.0 x 10^9 Pa	1.56 x 10^6 psi	2.0 x 10^9 Pa	66.6 x 10^9 Pa	63.0 x 10^9 Pa	47.5 x 10^9 Pa
Shear modulus, G_{12}, G_{13}	25.94 x 10^9 Pa	7.6 x 10^9 Pa	7.1 x 10^9 Pa	0.82 x 10^6 psi	0.775 x 10^9 Pa	25.6 x 10^9 Pa	24.8 x 10^9 Pa	3.75 x 10^9 Pa
Shear modulus, G_{23}	25.94 x 10^9 Pa	7.6 x 10^9 Pa	2.5 x 10^9 Pa	0.49 x 10^6 psi	0.775 x 10^9 Pa	25.6 x 10^9 Pa	24.8 x 10^9 Pa	1.3 x 10^9 Pa
Poisson's ratio, υ_{12}, υ_{12}	0.33	0.28	0.3	0.24	0.0	0.3	0.28	0.3
Piezoelectric stress constants,								
e_{31} (d_{31})	-	-	-	-	0.046 C/m^2	-215.0 x 10^{-12} C/N	166.0 x 10^{-12} m/V	192.0 x 10^{-12} m/V
e_{32} (d_{32})	-	-	-	-	0.046 C/m^2	-215.0 x 10^{-12} C/N	166.0 x 10^{-12} m/V	≈ 0.0 m/V
Dielectric permittivity,								
p_{11}, p_{22}, p_{33}	-	-	-	-	1.062 x 10^{-10} F/m	1.8585 x 10^{-8} F/m	15.2 x 10^{-9} F/m	-
Ply thickness, h_i	-	-	0.00125 m/ply	0.005 in/ply	0.0005 m	0.001 m	0.00025 m	0.00025 m
Length, a	0.25 m	0.25 m	0.25 m	9.0 in	0.1 m	0.25 m	0.25 m	0.25 m
Width, b	0.01 m	0.01 m	0.25 m	5.0 in	0.005 m	0.01 m	0.25 m	0.25 m